

8-15-2010

Comprehensive Reduced-Order Models Of Electrostatically Actuated MEMS Switches And Their Dynamics Including Impact And Bounce

Michael G. Snow

Purdue University - Main Campus, msnow@purdue.edu

Anil K. Bajaj

Purdue University - Main Campus, anil.k.bajaj.1@purdue.edu

Follow this and additional works at: <http://docs.lib.purdue.edu/prism>



Part of the [Nanoscience and Nanotechnology Commons](#)

Snow, Michael G. and Bajaj, Anil K., "Comprehensive Reduced-Order Models Of Electrostatically Actuated MEMS Switches And Their Dynamics Including Impact And Bounce" (2010). *PRISM: NNSA Center for Prediction of Reliability, Integrity and Survivability of Microsystems*. Paper 21.

<http://docs.lib.purdue.edu/prism/21>

This document has been made available through Purdue e-Pubs, a service of the Purdue University Libraries. Please contact epubs@purdue.edu for additional information.

DETC2010/MECH-28590

COMPREHENSIVE REDUCED-ORDER MODELS OF ELECTROSTATICALLY ACTUATED MEMS SWITCHES AND THEIR DYNAMICS INCLUDING IMPACT AND BOUNCE

Michael G. Snow

School of Mechanical Engineering
Purdue University
West Lafayette, Indiana 47907
msnow@purdue.edu

Anil K. Bajaj*

School of Mechanical Engineering
Purdue University
West Lafayette, Indiana 47907
bajaj@ecn.purdue.edu

ABSTRACT

As MEMS technology develops it is becoming better understood that MEMS designers must account for the large uncertainties characteristic of the relevant manufacturing processes. Uncertainty quantification tasks the designer with evaluating many different possible outcomes from the manufacturing process which creates a demand for models that are accurate and comprehensive, yet fast to evaluate. This work presents a comprehensive reduced-order model of electrostatically actuated switches incorporating a range of effects that are typically included only in FE modeling codes. Specifically, the model accounts for variable electrode geometry, stretching of centerline or large displacement effects, fringing field, squeeze film and rarefied gas damping, and allows for elastic contact with the dielectric substrate. Individual compact models for each of these effects are taken from literature and included in the model for the system. The dielectric substrate is modeled as an elastic foundation. The resulting partial differential equation for the switch modeled as a beam is discretized via a Galerkin method into ordinary differential equations for modal amplitudes. The Galerkin method uses the linear un-damped mode shapes of the beam to approximate the solution. Both cantilever and fixed-fixed type switches are analyzed. Static equilibrium solutions as a function of the applied voltage are developed along with their stability. Static pull-in voltages, first time of switch closure, and voltage for lift-off are studied with the model. To capture the contact

dynamics, the contact condition is evaluated with the substrate divided into a large number of elements and the contact force is projected on to the beam basis functions. In the case of cantilever geometry and slow voltage variations, three stable regimes of contact configuration and hysteresis between them are demonstrated.

NOMENCLATURE

A	Area of beam section
b	Beam width
E	Young's modulus of beam
E_f	Young's modulus of dielectric film
g_0	Equivalent Initial gap ($t_{air} + t_d/\epsilon_r$)
g	Instantaneous gap ($g_0 - w$)
h	Beam thickness
I	2nd moment of inertia
L	Beam Length
N	Residual tension
t_{air}	Air layer thickness
t_d	Dielectric thickness
V	Voltage
w	Beam displacement
λ	Gas mean free path

*Address all correspondence to this author.

INTRODUCTION

MEMS have had a large impact on industry as well as academia. Their marriage of different disciplines into unique devices has resulted in some exceptional performances as well as much exciting research potential. In the RF community, although it is by no means the only actuation scheme, electrostatic actuation has appeared as one of the most common means of actuations due to its relative simplicity in implementation. The force created by the attraction of opposite charges is well known but infrequently felt at the macro-scale, yet its length-scale dependence is such that it can be very effective at the micro-scale. The RF MEMS community has been very creative with the huge range of device designs [1–3], yet the simple geometries of a fixed-fixed beam and a cantilever beam have remained popular, again due to their relative simplicity in implementation. As such, the electrostatically actuated micro beam has become a topic frequented by researchers and covered by many works [4,5] including this one.

In the case of the capacitive switch design the beam acts as flexible electrode of a capacitor. DC bias across the system causes deflection of the beam, a thinner capacitor, an increased capacitance, and ultimately a collapse of the beam onto the other electrode, which must be protected by a dielectric insulator to prevent a short circuit. This collapse is called the pull-in phenomenon, it occurs when the linear elastic restoring force of the beam can no longer resist the $1/g^2$ electrostatic force. The voltage when this phenomenon occurs is the pull-in voltage and predicting it has been of enormous interest as some devices, such as switches must function above this voltage and others such as resonators, mixers, microphones etc. must not reach this voltage [6]. In addition to this unique instability there are a variety of other phenomena that have been the subject of much research.

Dynamic pull-in takes on two definitions in the literature. Nayfeh et al. [7] uses dynamic pull-in to refer to pull-in by a resonance phenomenon where the beam is oscillated via a mixed-signal AC+DC voltage. The second meaning, which will be referred to as 'DC dynamic pull-in', is the effect of the beam being pulled-in by a DC voltage below the pull-in voltage predicted by static-equilibrium analysis. This occurs due to dynamic effects when an actuation voltage is increased quickly. This work will use 'DC dynamic pull-in' to mean the latter mode of operation.

The modeling of these electrostatically actuated devices started with the most basic lumped mass-spring model. This model can be appropriate for some devices that physically resemble it, but is infrequently used for beams without modification. As researchers realized that a beam system often could not be equated well to a one degree of freedom model, they resorted to continuous domain models and FEM codes. FEM codes can produce very accurate results but are more computationally expensive. Continuous domain models were simulated using finite difference methods as well as reduced-order methods. McCarthy et al. [8] used a central difference scheme to simulate a beam with point contacts. Younis et al. [9] produced a reduced-order

model for electrostatically actuated micro-beams and the present work heavily relies on their developments.

In the literature on MEMS, some works are focused on improving general models for these devices whereas others focused on specifics. A frequent modeling assumption in analytical models of MEMS is the parallel-plate approximation. This assumption does not consider the fringing electric field present at the edges of two capacitor plates. Batra et al. [10] and others [11] have developed more accurate models than the parallel plate assumption. Batra et al. [10] fit a compact model to extensive FEM simulation data arriving at a fringing field model that accounted for finite beam width as well as thickness. Accounting for fringing field lowers predictions of the pull-in voltage a few percent depending on the width of the beam. Another frequent modeling assumption is that of linear viscous damping (or quality factor), which while greatly simplifying and sometimes even being applicable is not entirely accurate. The squeezing nature of the movement of the beam results in high damping nearer contact. Similarly to the fringing field compact models, researchers have used experimental and simulation data to create compact expressions for damping coefficients [12, 13].

The goal of this work is to create a modeling framework that is comprehensive enough to incorporate many of the multi-physics phenomena present in order to accurately predict the behaviors discussed previously; pull-in, DC-dynamic pull-in, bi and tri-stable states etc, while taking advantage of the work that has been done to improve the details of MEMS modeling, all without having to resort to costly FEM packages. The relatively fast evaluation of a reduced-order model is enormously useful to iterate designs, perform optimization and uncertainty quantification, all of which require large numbers of model runs.

This paper is organized into three sections. The modeling section goes through in detail the construction and solution of a reduced-order model. Modeling subsections describe details for the incorporation of other compact models into a Galerkin method framework. The results section uses the model formulation in a variety of ways to predict some of the behavior described above. Static equilibrium and pull-in results are described for fixed-fixed and cantilever beams. Bi-stable and Tri-stable states for cantilever beams are demonstrated. Dynamic solutions are presented for DC-dynamic pull-in calculations. Results of the model are compared to known literature. The conclusions section summarizes the work

MODELING OF THE MEMS SWITCH

Beam equation: The modeling process begins with the equation of motion for a fixed-fixed beam. Both fixed-fixed and cantilever beams are considered here and Fig. 1 shows the system(s) under consideration. As the cantilever case is a simplification of the fixed-fixed case, the model equations for the fixed-fixed are shown and the simplification to the cantilever case will

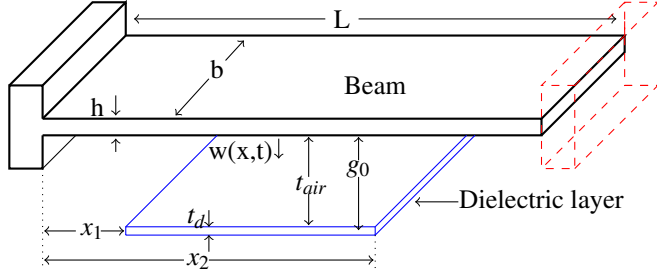


FIGURE 1. BEAM MODEL OF AN ELECTROSTATICALLY ACTUATED SWITCH.

be described later. The equation of motion for transverse vibration of a fixed-fixed beam which carries some residual axial load, and undergoes stretching is as follows [9]:

$$EI \frac{\partial^4 w}{\partial x^4} + \rho b h \frac{\partial^2 w}{\partial t^2} + F_{damp} = \left[\frac{EA}{2L} \int_0^L \left(\frac{\partial w}{\partial x} \right)^2 dx + \hat{N} \right] \frac{\partial^2 w}{\partial x^2} + F_{elec} + F_{contact} \quad (1)$$

where the electrostatic, the damping and the contact forces are included. The terms in (1) are, in order: restorative bending force, inertia, damping, stretching plus residual force, electrostatic force and contact force. Recognize that the stretching term is the binomial approximation for the change in arclength. Models for the damping, electrostatics, and contact are considered next.

Damping model: The damping due to the squeezing of the gas between the substrate and the beam can be considerably more than if the beam were moving in an unconfined medium. This has been extensively studied [12–15]. The model by Guo and Alexeenko [12] is used here. They have modeled the squeeze film effect as a linear viscous damping where the coefficient of damping varies with the beam displacement. Thus,

$$F_{damp} = c_f(w) \dot{w}. \quad (2)$$

The damping coefficient is given as:

$$c_f = \frac{10.39 \left(\frac{b}{t_{air} - w} \right)^{3.1}}{1 + 1.374 \left(\frac{b}{t_{air} - w} \right)^{1.825} \frac{\lambda}{b}^{0.966}} t. \quad (3)$$

Note that the model is a velocity proportional damping model where the damping coefficient depends on the gap-separation. Thus, the damping force is really a nonlinear function of beam displacement and velocity. For now the notation is simply $c_f(w)$.

Electrostatics Force Model: The force between the electrode and the beam is generally modeled via the model of a parallel plate capacitor. A parallel plate capacitor has the well known capacitance relation

$$C = \frac{\epsilon_0 A}{g}. \quad (4)$$

To find the force, the energy stored in a parallel plate capacitor is differentiated with respect to the separation between the plates. The energy is

$$E = \frac{1}{2} C V^2. \quad (5)$$

Differentiating this with respect to g yields the force between the plates of a parallel plate capacitor,

$$F = \frac{\epsilon_0 A V^2}{2g^2} \quad (6)$$

where the force is attractive. The accuracy of the parallel plate assumption is directly related to width of the beam. A wider beam will better approximate a parallel plate. A narrower beam will have a significant portion of its electric field emanating from its sides and top of the beam, making a parallel plate model inappropriate. Incorporating a model for this fringing field makes this formulation more accurate. Batra et al. [10] modeled the capacitance of a narrow microbeam with a modifying factor to the basic parallel plate model. This was a fit to results derived from finite element simulations of the electrostatics problem. Thus,

$$C = \frac{\epsilon_0 A}{g} P(w) \quad (7)$$

where

$$P(w) = 1 - 0.36 \frac{1}{b} (g_0 - w) + \left(0.85 \frac{1}{b^{0.76}} + 2.5 \frac{h^{0.24}}{b} \right) (g_0 - w)^{0.76}. \quad (8)$$

The force is found by differentiating in the same manner as above, which yields the force

$$F_{elec} = \frac{\epsilon_0 b V^2}{2(g_0 - w)^2} \left(1 + 0.24 A_0 (g_0 - w)^{0.76} \right) \quad (9)$$

where

$$A_0 = \left(0.85 \frac{1}{b^{0.76}} + 2.5 \frac{h^{0.24}}{b} \right). \quad (10)$$

Impact Model: A soft contact model is employed here. The impacted substrate acts as a stiff, distributed spring and thus the contact term in the equation of motion is defined as:

$$F_{contact} = -\frac{E_f b}{t_d}(w - t_{air})(w \geq t_{air}). \quad (11)$$

It should be noted that in this analysis, g_0 is the equivalent initial gap and that impact occurs before $w = g_0$, ($g_0 = t_{air} + t_d/\epsilon_r$). Thus impact will occur before the singularity in the electrostatic force. Also, as we have defined the attraction of the beam to the electrode as the positive direction, hence the minus sign in the contact force expression.

The Equation of Motion

Combining (9), (11) and (2) into (1) yields the beam's equation of motion:

$$EI \frac{\partial^4 w}{\partial x^4} + \rho b h \frac{\partial^2 w}{\partial t^2} + c_f(w) \frac{\partial w}{\partial t} = \left[\frac{EA}{2L} \int_0^L \left(\frac{\partial w}{\partial x} \right)^2 dx + \hat{N} \right] \frac{\partial^2 w}{\partial x^2} + \frac{\epsilon b v^2(t)}{2(g_0 - w)^2} P(w) + \frac{E_f b}{t_d}(w - t_{air})(w \geq t_{air}). \quad (12)$$

Note that the explicit forms for $c_f(w)$ and $P(w)$ have been left out, this will be addressed later.

Non-dimensionalization: The non-dimensional variables:

$$\hat{x} = \frac{x}{L} \quad \hat{w} = \frac{w}{g} \quad \hat{t} = \frac{t}{T} \quad (13)$$

serve to make the equations more manageable. Substituting the non-dimensionalized, length, displacement, and time yields the non-dimensionalized equation of motion for the beam. This equation is:

$$\frac{\partial^4 \hat{w}}{\partial \hat{x}^4} + \frac{\partial^2 \hat{w}}{\partial \hat{x}^2} + c \frac{\partial \hat{w}}{\partial \hat{t}} = [\alpha_1 \Gamma(\hat{w}, \hat{w}) + \hat{N}] \frac{\partial^2 \hat{w}}{\partial \hat{x}^2} + \frac{\alpha_2 v^2(t)}{(1 - \hat{w})^2} (1 + A_1(1 - w)^{0.76}) + \alpha_3 (\hat{w} \geq \frac{g_0 - t_{air}}{g_0}) (\hat{w} - \frac{g_0 - t_{air}}{g_0}) \quad (14)$$

where

$$\alpha_1 = 6 \left(\frac{d}{h} \right)^2 \quad c = \frac{\hat{c}(w)L^4}{EIT} \quad \hat{N} = \frac{NL^2}{EI} \quad A_1 = 0.24A_0 g_0^{0.76} \\ \alpha_2 = \frac{6\epsilon_0 L^2}{Eh^3 d^3} \quad \alpha_3 = \frac{E_f L^4 b}{t_d EI} \quad T = \sqrt{\frac{\rho b h L^4}{EI}} \quad (15)$$

and the function Γ is expressed

$$\Gamma(f_1(x, t), f_2(x, t)) = \int_0^1 \frac{\partial f_1}{\partial x} \frac{\partial f_2}{\partial x} dx. \quad (16)$$

Hats are dropped from this point forward for convenience.

Finite Electrode Width Case: Most MEMS beams do not have actuation electrodes that span to whole length of the beam. The model in equation (12) is written as if this is the case. Step functions to indicate the start and end of the actuation electrode along the beam in the x-direction serve this purpose. The new non-dimensionalized equation of motion is thus:

$$\frac{\partial^4 w}{\partial x^4} + \frac{\partial^2 w}{\partial x^2} + c \frac{\partial w}{\partial t} = [\alpha_1 \Gamma(w, w) + N] \frac{\partial^2 w}{\partial x^2} + \frac{\alpha_2 v^2(t)}{(1 - w)^2} (1 + A_1(1 - w)^{0.76}) (H(x - x_1) - H(x - x_2)) + \alpha_3 (w \geq \frac{g_0 - t_{air}}{g_0}) (w - \frac{g_0 - t_{air}}{g_0}) \quad (17)$$

where x_1 is the fraction of the beam before the electrode starts, and x_2 is the fraction of the beam before the electrode ends. For example, if the electrode occupies the center third of the beam then $x_1 = 1/3$ and $x_2 = 2/3$. While the fringing field that occurs between the sides of the beam and the top plate of the actuation electrode have been modeled there is another fringing field between the sides of the electrode and the bottom plate of the beam. By using step function to cut off the electrostatic force at the ends of the electrode, this fringing field has not been taken into account. For most switch geometries the fringing field from beam sides to electrode top occurs over a greater length than that between the electrode sides and beam bottom and as such is a more significant effect.

SOLUTION METHODOLOGY

In order to solve the beam model (17), it is assumed that the solution at any given time is a linear combination of the linear modeshapes of the undamped, undeflected microbeam. The

solution then takes the form

$$w(x,t) = \sum_{i=1}^M u_i(t) \phi_i(x) \quad (18)$$

where $\phi_i(x)$ is the i th linear undamped mode shape of the beam with appropriate boundary conditions and u_i are time varying coefficients. The mode shapes are the solution to the equation:

$$\phi_i^{iv} = N\phi_i'' + \omega_i^2 \phi_i \quad (19)$$

and the boundary conditions (for a fixed-fixed beam)

$$\phi_i(0) = 0 \quad \phi_i(1) = 0 \quad \phi_i'(0) = 0 \quad \phi_i'(1) = 0. \quad (20)$$

The modeshapes are also normalized to obey the orthogonality property

$$\int_0^1 \phi_i \phi_j dx = \delta_{ij}. \quad (21)$$

There exist closed-form expressions for the modal frequency equations and modeshapes in literature. The formulas for a cantilever beam can be found in Rao [16], and many other sources. The closed form expressions for a fixed-fixed beam under axial tension can be found in Shaker [17].

Galerkin Method

To solve the beam model using modal superposition we substitute the expansion (18) into equation (17), multiply through by $(1-w)^2$ to get rid of rational terms, multiply by ϕ_n and finally use the orthogonality property by integrating everything from 0 to 1. However a difficulty appears with $c(w)$ and $P(w)$; they are not in integer powers of w and there is not a good way to express a fractional power of a series. This is rectified by starting over and expressing $c(w)$ and $P(w)$ as Taylor Polynomials.

Taylor Expansion of Fringing Field Model: The dimensional electrostatic force (9) can be non-dimensionalized to

$$F_{elec} = \frac{\epsilon_0 b V^2}{2g_0^2 (1-w)^2} (1 + A_1 (1-w)^{0.76}) \quad (22)$$

where:

$$A_1 = .204 \left(\frac{g_0}{b} \right)^{0.76} + .6 \frac{h^{.24} g_0^{0.76}}{b}. \quad (23)$$

The 3rd order Taylor expansion of this is

$$F_{elec} \approx \frac{\epsilon_0 b V^2}{2g_0^2 (1-w)^2} (1 + A_1 - 0.76A_1 w - 0.0912A_1 w^2 - 0.0377A_1 w^3) \quad (24)$$

The form of equation (24) is now suitable for the Galerkin method. Note that the error between F_{elec} in (22) and its approximation (24) is less than 1.5% over the range of $0 \leq w \leq 1$ for $A_1 = .1$. A similar method is used to express the damping coefficient.

Taylor Expansion of the Damping Coefficient: The damping model of Guo and Aleexenko [12] was included in a similar fashion. Starting with equation (3) and assigning some factors the damping model becomes

$$c_f = \frac{B_1 g^{-3.1}}{1 + B_2 g^{-1.825}} \quad (25)$$

where $B_1 = 10.396b^{3.1}t$ and $B_2 = 1.374b^{1.825} \left(\frac{\lambda}{b} \right)^{0.966}$. Manipulating g results in

$$c_f = g^{-2} \frac{B_1 g^{.725}}{B_2 + g^{1.825}} \quad (26)$$

Some additional algebraic manipulation results in

$$c_f = (1-w)^{-2} \frac{B'_1 (1-w)^{.725}}{B'_3 (1-w)^{1.825} + B'_2} \quad (27)$$

where the new parameters are:

$$\begin{aligned} B'_1 &= 10.39b^{3.1}t g_0^{-1.275} \\ B'_2 &= 1.374b^{1.825} \left(\frac{\lambda}{b} \right)^{0.966} \\ B'_3 &= g_0^{1.825}. \end{aligned} \quad (28)$$

The first $(1-w)^{-2}$ in equation (27) will be eliminated when the whole equation of motion is multiplied by $(1-w)^2$. The remainder of the damping term we can expand in a Taylor series

to give:

$$c_f \approx (1-w)^{-2} \left(\left(\frac{B'_1}{B'_2 + B'_3} \right) + \left(\frac{-0.725B'_1(B'_2 - 1.5172B'_3)}{(B'_2 + B'_3)^2} \right) w + \left(\frac{-0.0997B'_1(B'_2^2 + 22.8245B'_2B'_3 - 11.5862B'_3^2)}{(B'_2 + B'_3)^3} \right) w^2 \right). \quad (29)$$

To ultimately express this model in a compact form some additional factors were assigned:

$$\begin{aligned} C_1 &= \left(\frac{B'_1}{B'_2 + B'_3} \right) \\ C_2 &= \left(\frac{-0.725B'_1(B'_2 - 1.5172B'_3)}{(B'_2 + B'_3)^2} \right) \\ C_3 &= \left(\frac{-0.0997B'_1(B'_2^2 + 22.8245B'_2B'_3 - 11.5862B'_3^2)}{(B'_2 + B'_3)^3} \right). \end{aligned} \quad (30)$$

Ultimately the desired polynomial form

$$c_f \approx (1-w)^{-2} (C_1 + C_2 w + C_3 w^2) \quad (31)$$

is obtained for the damping coefficient. The factor $(1-w)^2$ in (31) will be eliminated when following the solution procedure detailed above.

Solution Procedure

First the modified damping form in equation (31) and fringing field model in equation (24) are substituted back into equation (17). Now multiplying by $(1-w)^2$ leaves only integer powers of the displacement w and thus the modal expansion (18) can be substituted. After these steps are taken, the resulting equation is finally broken down into a set of ODEs in time for each modal amplitude u_i . This is done by multiplying by ϕ_n and integrating from zero to one. This last step exploits (21) and yields the set of ODEs

$$\begin{aligned} \ddot{u}_n - 2 \sum_{i,j=1}^M \ddot{u}_i u_j \int_0^1 \phi_i \phi_j \phi_n dx \\ + \sum_{i,j,k=1}^M \ddot{u}_i u_j u_k \int_0^1 \phi_i \phi_j \phi_k \phi_n dx = \\ - C_1 \dot{u}_n - \omega_n^2 u_n \\ - C_2 \sum_{i,j=1}^M \dot{u}_i u_j \int_0^1 \phi_i \phi_j \phi_n dx \end{aligned}$$

$$\begin{aligned} - C_3 \sum_{i,j,k=1}^M \dot{u}_i u_j u_k \int_0^1 \phi_i \phi_j \phi_k \phi_n dx \\ + 2 \sum_{i,j=1}^M u_i u_j \omega_i^2 \int_0^1 \phi_i \phi_j \phi_n dx \\ - \sum_{i,j,k=1}^M u_i u_j u_k \omega_i^2 \int_0^1 \phi_i \phi_j \phi_k \phi_n dx \\ + \alpha_1 \sum_{i,j,k=1}^M u_i u_j u_k \Gamma(\phi_i, \phi_j) \int_0^1 \phi_k'' \phi_n dx \\ - 2\alpha_1 \sum_{i,j,k,l=1}^M u_i u_j u_k u_l \Gamma(\phi_i, \phi_j) \int_0^1 \phi_k'' \phi_l \phi_n dx \\ + \alpha_1 \sum_{i,j,k,l,m=1}^M u_i u_j u_k u_l u_m \Gamma(\phi_i, \phi_j) \int_0^1 \phi_k'' \phi_l \phi_m \phi_n dx \\ + \alpha_2 v^2(t) (A_1 + 1) \int_{x_1}^{x_2} \phi_n dx \\ + \alpha_2 v^2(t) (-0.76A_1) \sum_{i=1}^M u_i \int_{x_1}^{x_2} \phi_i \phi_n dx \\ + \alpha_2 v^2(t) (-0.0912A_1) \sum_{i,j=1}^M u_i u_j \int_{x_1}^{x_2} \phi_i \phi_j \phi_n dx \\ + \alpha_2 v^2(t) (-0.0377A_1) \sum_{i,j,k=1}^M u_i u_j u_k \int_{x_1}^{x_2} \phi_i \phi_j \phi_k \phi_n dx \\ + \int_0^1 -k(w - t_{air})(w \geq t_{air}) (1-w)^2 \phi_n dx, \end{aligned} \quad (32)$$

for $n=1,2,\dots,M$.

There are some things worth pointing out in equations (32). First, note that the set of equations is $O(M^6)$ (M equations containing M^5 terms) meaning that computational cost increases dramatically with the number of modes. Second, note the appearance of x_1 and x_2 in the integration limits of the voltage terms; this is a natural simplification of integrating over step functions. Finally, note that the modal expansion was not applied to the impact term. This arises from the conditional coefficient ($w \geq t_{air}$) which can not be easily expressed in terms of modeshapes. Checking for contact requires reassembling w via (18) at every time step and checking for interference with the dielectric.

Cantilever Case: A Cantilever beam can be modeled with the same methodology. To model a cantilever the pre-tension N and stretching term coefficient α_1 are set to zero and the appropriate boundary conditions are used for finding the mode shapes ϕ_n . It should be noted that the resulting simplification to (32) is the loss of the highest order terms. These terms are due to the stretching non-linearity and the result is that the cantilever case is $O(M^4)$ (M equations containing M^3 terms) and

generally much faster to evaluate than the fixed-fixed case.

EQUILIBRIUM AND STATIC PULL-IN PREDICTIONS

Static solutions to equations (32) are explored first. The method used to find the static solutions is an enforced displacement scheme. The static solutions are found by eliminating the dynamic terms in (32) and using the remaining expressions as measures of error. An addition error measure is obtained from the distance from a desired displacement at a given point along the beam; say at the mid-point for example. Thus, $(M + 1)$ equations are to be satisfied or $(M + 1)$ errors must be zero, that is, when a trial solution of M modal amplitudes and a voltage is plugged into the error measures and the errors are all zero, the trial solution is a static solution. Starting from a non-static guess solution, we can obtain the partial derivatives of the error measures with respect to each modal amplitude and the voltage. Using a Jacobian matrix constructed from these partial derivatives, an iterative Newton-Raphson scheme updates the guess solution until all the error measures are sufficiently small. By slowly stepping through the desired displacements from zero up to contact, the static solution curves are obtained. It should be noted that the solutions found by this technique are unique except in cases of buckled modes. For a fixed-fixed beam the displacement was enforced at the midpoint with the equilibrium voltage solved for from zero displacement up to contact. For a cantilever beam it is informative to enforce displacements at the tip as well as other points on the beam. Enforcing displacements at the midpoint of the cantilevers shows some post-contact phenomena including tri-stable configurations, i.e. three distinct configurations of the beam for a given voltage.

The results for a prototypical cantilever beam; $L = 350\mu$, $b = 40\mu$, $h = 2\mu$, $d = 2\mu$, $E = 169GPa$, $\nu = .06$, $x_1 = 0, x_2 = 0$ are shown in Fig. 2 for up to 10 modes. The highest voltage on the plot, the locally vertical point of the curve where it changes from the stable lower branch ($\frac{dw}{dx} \geq 0$) to the unstable upper branch ($\frac{dw}{dx} < 0$) is dubbed the static pull-in voltage. For these dimensions, using 5-10 modes, the static pull in voltage is predicted at 4.705Volts. Generally, as the number of modes increases, the model converges very quickly for low displacements and slower for high displacements. Three modes are often sufficient for predicting the pull-in voltage, while predicting the release voltage requires at least 5 modes. Thin dielectrics, unusual electrode set-ups and post-contact predictions take a significant number of modes.

The static displacement for a fixed-fixed beam will appear qualitatively similar to the cantilever data in Fig. 2. The fixed-fixed beam of otherwise equivalent dimensions will obviously have a much higher pull-in voltage, otherwise the graph will appear similar. The maximum stable displacement, however, may be larger as the stretching in a fixed-fixed beam may result in stability closer to the electrode. There is however addition inter-

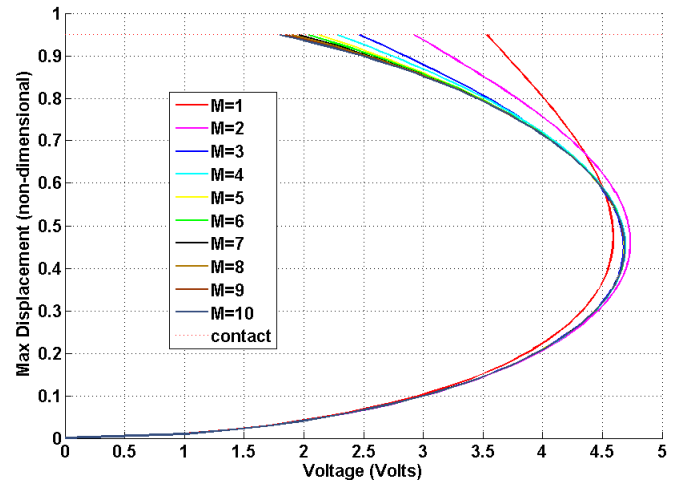


FIGURE 2. CONVERGENCE OF STATIC SOLUTIONS FOR A CANTILEVER BEAM.

esting behavior in the cantilever system that is not revealed by Fig. 2.

Enforcing displacements at the midpoint of a cantilever beam reveals three stable states, before pull-in, pinned at the tip, and flat. In line with [18], there is hysteresis between the three states and they can be seen in the transitions between the stable branches ($\frac{dw}{dx} \geq 0$) of Fig. 3 which displays the relationship between the static displacement of the midpoint of a cantilever and the voltage. The arc from zero displacement up to $w = 0.3$ corresponds to the pre-contact deflection of the beam. At $w = 0.3$ the tip of the cantilever is in contact, hence the low voltage. The next arc in the curve corresponds to the transition from pinned-tip contact to flat contact. The convergence on this section of the curve is much slower as parts of the beam are in contact. In the last section of the curve, from $w = .55$ to $w = 1$ the voltage increases sharply until the midpoint of the beam is brought into contact, again the convergence is slow due to much of the beam being in contact. Excluding dynamic effects, slowly increasing the voltage would cause the beam to transition to tip-contact at 4.7 volts, and flat contact at approximately 6 volts. Lowering the voltage from this point would cause the beam to transition from flat contact to pinned contact at approximately 4 volts and eventually release at approximately 2 volts.

When calculating the mode shapes of the Euler-Bernoulli beam in MATLAB a subtle problem arises in 11 or 12th mode shapes. Even when using double-precision variables enormous rounding errors appear and the conventional formulas don't yield usable results beyond the 11th mode. This is due to $\cosh()$ and $\sinh()$ terms which are very large and nearly equal. When these terms are subtracted nearly all the significant digits are

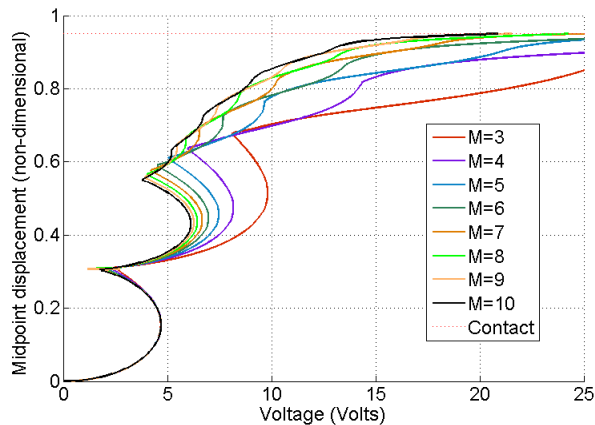


FIGURE 3. BEAM MIDPOINT STATIC SOLUTIONS FOR A CANTILEVER BEAM.

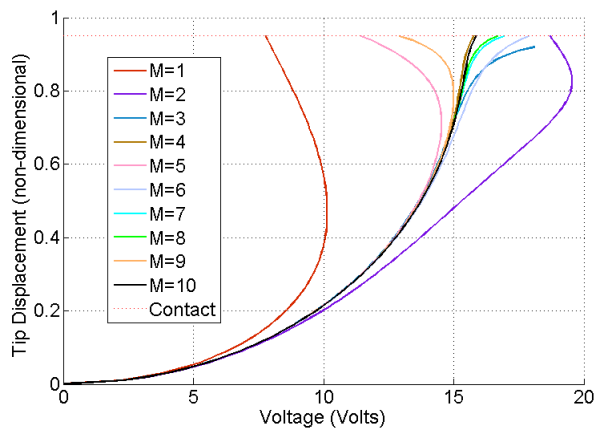


FIGURE 4. CONVERGENCE OF STATIC SOLUTIONS ($x_2 = 0.55$) FOR A CANTILEVER.

lost. Gonçalves et al. [19] solved this with some clever algebraic manipulations and using his technique higher-order modes than 10 could be used. Although the solutions with greater than 10 modes have not been plotted they have been shown to converge.

Another interesting case is the analysis of an electrode design to reduce or eliminate the static pull-in instability. The concept is that by shortening the electrode such that $x_1 = 0$ and $x_2 \approx 0.5$ the beam's tip will make contact before the beam section that is actually above the electrode gets too close. Ideally, this eliminates the hysteresis and pull-in effects found in the nominal case. A test case with the same parameters (with the exception that $x_2 = 0.55$) as used previously is shown in Fig. 4. Again the convergence is slow near contact, and while not quantitatively converged, the graph shows the expected behavior quite

TABLE 1. Pull-in voltage comparisons for Cantilevers.

Parameters: $E=77\text{GPa}$, $\nu = .33$, $h=3\mu\text{m}$, $g_0=1\mu\text{m}$

Variables	Case 1	Case 2	Case 3
$L(\mu\text{m})$	300	500	300
$b(\mu\text{m})$	50	50	0.5
V_{PI} [21]	2.33	0.84	1.33
V_{PI} [22]	2.27	0.8180	1.23
V_{PI} CW FEA	2.25	0.75	1.20
V_{PI} Compact model [20]	2.27	0.8188	1.21
V_{PI} This model	2.258	0.8131	1.207

well. The one-to-one relationship between static tip-deflection and voltage means that there are no unstable branches and no hysteresis when actuating the switch, it releases at the same voltage it pulls-in.

In order to verify that the fully converged model was accurate, prediction of pull-in voltages were compared against some available experiments and other published models. The results in Table 1 are from [20] with results from this work included. Experimental results are taken from Pamidighantam et al. [21] and Osterberg [22].

DYNAMIC SOLUTIONS

Dynamic solutions to equations (32) are found by direct time integration in MATLAB. The ODE23s routine was used to perform the integration as the equations become somewhat stiff near and after contact. It is well understood that MEMS beams can pull-in at voltages under their static pull-in voltage due to dynamic effects. A beam can be given enough momentum by a lower voltage to carry it past its static equilibrium solution to pull-in. The lower limit of voltage when pull-in occurs due to this dynamic effect is called the DC-dynamic pull-in. This is typically around 8% lower than the static pull-in voltage [23]. This is found with this model by a bi-section search method. Applying a step input voltage (or a given rise time) much lower than the static pull-in voltage where the beam does not pull-in and a much higher voltage that causes pull-in creates a window of voltages that contains the DC-dynamic pull-in voltage. The bisection search proceeds to divide the search interval by applying the voltage in the middle of the window, integrating in time under these conditions, and observing whether or not the beam pulls-in, and appropriately choosing a half-window to call the new window and dividing again. The process is carried out until the window is of some acceptably small width, such as 10mV. The process is illustrated in Fig. 5 where the bisection search history is shown for

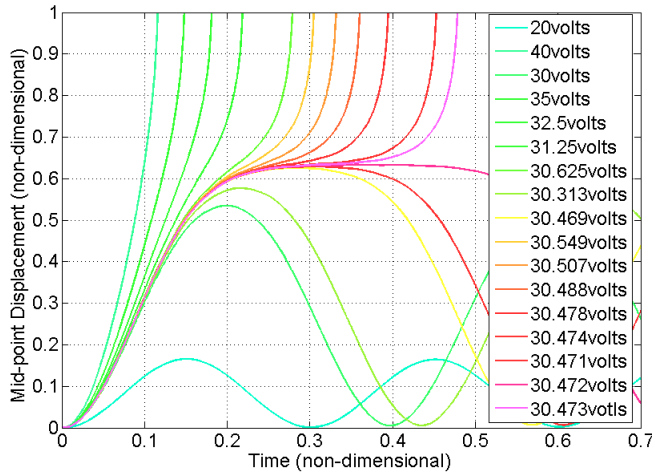


FIGURE 5. CONVERGENCE OF BISECTION SEARCH FOR EVALUATING THE DYNAMIC PULL-IN OF A FIXED-FIXED BEAM.

a fixed-fixed beam. Parameters in Fig. 5 are $L = 350\mu$, $b = 40\mu$, $h = 2\mu$, $d = 2\mu$, $E = 169GPa$, $v = 0$, $x_1 = 0.2$, $x_2 = 0.8$, $\frac{\lambda}{b} = 1$ and $M = 5$. For these parameters, the DC-dynamic pull-in voltage is 30.47 volts. Comparing this to the predicted static pull-in voltage, 33.33 volts, it is 8.6% lower, as expected. In Fig. 5 the frequency of the oscillatory response can be seen to decrease as the actuation voltage increases. This is due to the softening effect of the electrostatic force. When α_1 is large it is possible to see an increase in frequency followed by a decrease. In general the closing time becomes large as the DC-dynamic pull-in voltage is approached. The DC-dynamic pull-in voltage will drive the beam to near-rest on the unstable branch with minute differences in voltage determining whether the beam oscillates or impacts. This near-rest effect is significant when within roughly 10mV of the true DC-dynamic pull-in voltage. It should also be said that computing the DC-dynamic pull-in voltage to this fine accuracy is of little help to the designer or engineer as other modeling, manufacturing or experimental uncertainties will dominate.

The DC-dynamic pull-in calculations can be done entirely without contact dynamics. As mentioned previously, the model converges slower near and post contact. Although it is difficult to ensure that the contact dynamics are being calculated accurately it is possible to get a good qualitative understanding of the contact behavior. An example of bouncing of a fixed-fixed beam during actuation is given in Fig. 6. The parameters are those used in figure 5 and the actuation voltage is a step voltage slightly above the dynamic pull-in voltage. The line colors and thicknesses in the plot are only for visual aid. Each snapshot is roughly equally spaced in time.

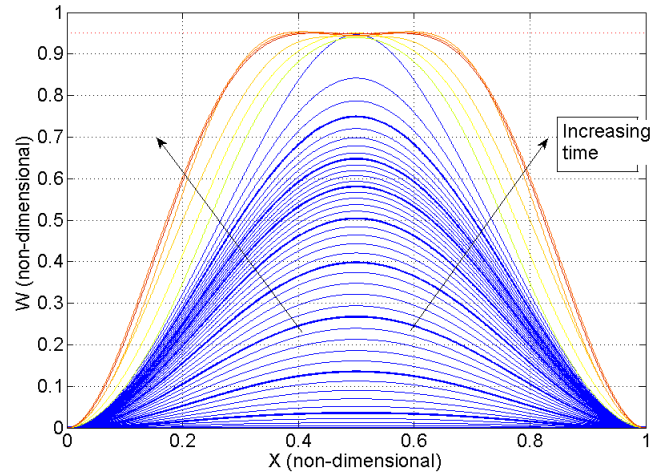


FIGURE 6. SNAP SHOTS OF A FIXED-FIXED BEAM BOUNCING AGAINST THE SUBSTRATE.

CONCLUSIONS

A comprehensive model was effective in predicting the different quantitative and qualitative behaviors of beam-type electrostatically actuated switches. A model that quickly predicts the behavior of a MEMS beam under a variety of conditions will prove valuable in tackling looming problems in the MEMS community which require many model evaluations, such as for uncertainty quantification. The model does have some shortcomings, the worst of which is the slow convergence near contact which occurs both near and during contact. The ODEs in the reduced-order model (32) are very complicated and beyond a certain number of modes any computational benefits may be lost. Then it would be advantageous to switch to a finite difference scheme. The damping model is accurate but was developed only with small oscillations in mind and was not designed for switches operating over a large vertical displacement. Near contact, the model is extrapolating from the damping model rather than interpolating. Perhaps the biggest effect not included in this model is the lack of any accounting for imperfect beam anchors or pre-distortion of the beam itself. However, the model is set-up in such a way that it is not difficult to incorporate such effects. As the model only depends on mode shapes and frequencies, imperfect anchors could be simulated in an FEM package to find equivalent beam end-conditions and these could be used to extract the appropriate mode shapes and frequencies to be inserted into the model. It may be possible to account for pre-distorted beams, such as arches, in a similar way. The model would also be well served by having more modeshapes beyond 11 or 12 to work with. Allowing the use of enough modes to accurately simulate contact would be valuable. The accurate calculation of contact stresses might lead to a computationally inexpensive damage

model as well. In the end the strength of this framework is its flexibility.

ACKNOWLEDGMENT

The work is supported by NNSA Center for Prediction of Reliability, Integrity and Survivability of Microsystems at Purdue University under contract number DE-FC52-08NA28617. Thanks go to Dr. Dimitri Peroulis for his invaluable discussion on MEMS design and experimental procedures. Thanks are also in order for Dr. Charles Tong of Lawrence Livermore National Laboratories. His mentorship on the subject of uncertainty quantification directed the focus of this model in a better direction.

REFERENCES

- [1] Joshi, H., Sigmarsson, H., Moon, S., Peroulis, D., and Chappell, W., 2009. "High- q fully reconfigurable tunable bandpass filters". *Microwave Theory and Techniques, IEEE Transactions on*, **57**(12), Dec., pp. 3525–3533.
- [2] Vyas, A., and Bajaj, A., 2008. "Dynamics of a nonlinear microresonator based on resonantly interacting flexural-torsional modes". *Nonlinear Dynamics*, **54**(1), Jan., pp. 31–52.
- [3] Xie, Y., Li, S.-S., Lin, Y.-W., Ren, Z., and Nguyen, C.-C., 2008. "1.52-ghz micromechanical extensional wine-glass mode ring resonators". *Ultrasonics, Ferroelectrics and Frequency Control, IEEE Transactions on*, **55**(4), April, pp. 890–907.
- [4] Lin, X., and Ying, J., 2008. "Analytical model of electrostatic fixed-fixed microbeam for pull-in voltage". In *Advanced Intelligent Mechatronics, 2008. AIM 2008. IEEE/ASME International Conference on*, pp. 803–807.
- [5] Krylov, S., and Maimon, R., 2004. "Pull-in dynamics of an elastic beam actuated by continuously distributed electrostatic force". *Journal of Vibration and Acoustics*, **126**(3), pp. 332–342.
- [6] Rebeiz, G. M., 2003. *RF MEMS: Theory, Design, and Technology*. John Wiley & Sons, Inc., New York, NY, USA.
- [7] Nayfeh, A., Younis, M., and E., A.-R., 2007. "Dynamic pull-in phenomenon in mems resonators". *Nonlinear Dynamics*, **48**(1), Jan., pp. 153–163.
- [8] McCarthy, B., Adams, G., McGruer, N., and Potter, D., 2002. "A dynamic model, including contact bounce, of an electrostatically actuated microswitch". *Microelectromechanical Systems, Journal of*, **11**(3), Jun., pp. 276–283.
- [9] Younis, M., Abdel-Rahman, E., and Nayfeh, A., 2003. "A reduced-order model for electrically actuated microbeam-based mems". *Microelectromechanical Systems, Journal of*, **12**(5), Oct., pp. 672–680.
- [10] Batra, R., Porfiri, M., and Spinello, D., 2006. "Electromechanical model of electrically actuated narrow microbeams". *Microelectromechanical Systems, Journal of*, **15**(5), Oct., pp. 1175–1189.
- [11] Meijs, N., and Fokkema, J., 1984. "Vlsi circuit reconstruction from mask topology". *Integration*, **2**(2), pp. 363–366.
- [12] Guo, X., and Alexeenko, A., 2009. "Compact model of squeeze-film damping based on rarefied flow simulations". *Journal of Micromechanics and Microengineering*, **19**(4), p. 045026 (7pp).
- [13] Lee, J. W., Tung, R., Raman, A., Sumali, H., and Sullivan, J. P., 2009. "Squeeze-film damping of flexible microcantilevers at low ambient pressures: theory and experiment". *Journal of Micromechanics and Microengineering*, **19**(10), p. 105029 (14pp).
- [14] Steeneken, P. G., Rijks, T. G. S. M., van Beek, J. T. M., Ulenaers, M. J. E., Coster, J. D., and Puers, R., 2005. "Dynamics and squeeze film gas damping of a capacitive rf mems switch". *Journal of Micromechanics and Microengineering*, **15**(1), pp. 176–184.
- [15] Bao, M., and Yang, H., 2007. "Squeeze film air damping in mems". *Sensors and Actuators A: Physical*, **136**(1), pp. 3–27. 25th Anniversary of Sensors and Actuators A: Physical.
- [16] Rao, S., 2003. *Mechanical Vibration 4th ed.* Pearson Prentice Hall.
- [17] Shaker, F., 1975. Effect of axial load on mode shapes and frequencies of beams. Tech. rep., Lewis Research Center Report NASA-TN-8109, Dec.
- [18] Gorthi, S., Mohanty, A., and Chatterjee, A., 2006. "Cantilever beam electrostatic mems actuators beyond pull-in". *Journal of Micromechanics and Microengineering*, **16**(9), pp. 1800–1810.
- [19] Goncalves, P., Brennan, M., and Elliott, S., 2007. "Numerical evaluation of high-order modes of vibration in uniform euler-bernoulli beams". *Journal of Sound and Vibration*, **301**(3-5), pp. 1035–1039.
- [20] Chowdhury, S., Ahmadi, M., and Miller, W. C., 2005. "A closed-form model for the pull-in voltage of electrostatically actuated cantilever beams". *Journal of Micromechanics and Microengineering*, **15**(4), pp. 756–763.
- [21] Pamidighantam, S., Puers, R., Baert, K., and Tilmans, H. A. C., 2002. "Pull-in voltage analysis of electrostatically actuated beam structures with fixed-fixed and fixed-free end conditions". *Journal of Micromechanics and Microengineering*, **12**(4), pp. 458–464.
- [22] Osterberg, P., 1995. "Electrostatically acuated microelectromechanical test structures for material property measurements". Phd thesis, Massachusetts Institute of Technology, MA.
- [23] Chao, P. C.-P., Chiu, C. W., and Liu, T.-H., 2008. "Dynamic pull-in predictions for a generalized clamped-clamped micro-beam based on a continuous model and bifurcation analysis". *Journal of Micromechanics and Microengineering*, **18**(11), p. 115008 (14pp).